On the impact of wind on the development of wave field during storm Britta

Larsén, Xiaoli Guo; Du, Jianting; Bolaños, Rodolfo; Larsen, Søren

Published in:
Ocean Dynamics

Link to article, DOI:
10.1007/s10236-017-1100-1

Publication date:
2017

Document Version
Peer reviewed version

Ocean Dynamics manuscript No.
(will be inserted by the editor)

On the impact of wind on the development of wave field during storm Britta

Xiaoli Guo Larsén · Jianting Du · Rodolfo Bolaños · Søren Larsen

the date of receipt and acceptance should be inserted later

Abstract The observation of extreme waves at FINO 1 during storm Britta on the 1st November 2006 has initiated a series of research studies regarding the mechanisms behind. The roles of stability and the presence of the open cell structures have been previously investigated but not conclusive. To improve our understand-

Danish ForskEL project XWiWa PSO-12020

Xiaoli Guo Larsén

Wind Energy Department, Risø Campus of the Danish Technical University

Tel.: +45 2132 7332

E-mail: xgal@dtu.dk

Jianting Du

Wind Energy Department, Risø Campus of the Danish Technical University

Rodolfo Bolaños

DHI Water and Environment

Søren Larsen

Wind Energy Department, Risø Campus of the Danish Technical University

ing of these processes, which are essential for a good forecast of similarly important events offshore, this study revisits the development of storm Britta using an atmospheric and wave coupled modeling system, wind and wave measurements from 10 stations across the North Sea, cloud images and Synthetic Aperture Radar (SAR) data. It is found here that a standard state-of-the-art model is capable of capturing the important characteristics of a major storm like Britta, including the storm path, storm peak wind speed, the open cells and peak significant wave height (H_s) for open sea. It was also demonstrated that the impact of the open cells has negligible contribution to the development of extreme H_s observed at FINO 1. At the same time, stability alone is not sufficient in explaining the development of extreme H_s. The controlling conditions for the development of Britta extreme H_s observed at FINO 1 are the persistent strong winds and a long and undisturbed fetch over a long period.

Keywords Storm Britta · WRF · SWAN · Open cell

1 Introduction

Since the day it hit the North Sea on 1st Nov. 2006, storm Britta has become a research focus for both atmospheric and wave modeling, e.g. Brusch et al (2008); Behrens and Günther (2009); Pleskachevsky et al (2012); Kettle (2015b). At the same time, measurements have been analyzed extensively for understanding the development of this storm (e.g. Emeis and Türk (2009)). Storm Britta is characterized of strong and highly fluctuating mean wind speed and unusually high waves in the North Sea, where FINO 1 experienced a 20-year return value for the significant wave height and where structural damages on the FINO 1 platform

were reported at a 15 m tall working deck (Kettle 2015a). It also caused a remarkable storm surge on the coast of the Netherlands, Germany and the southern Baltic Sea (Kettle 2015b). This storm has attracted significant attention from the offshore wind industry, since a large number of offshore wind farms are planned in the southern North Sea where the design specifications for the offshore wind turbines outlined smaller extreme waves (Kettle 2016). Storm Britta emphasized the need for met-ocean community to understand the extreme waves observed in the southern North Sea.

In a series of studies of Britta, e.g., Brusch et al (2008), Behrens and Günther (2009), Emeis and Türk (2009), Pleskachevsky et al (2012) and Kettle (2015b), the following features have been observed:

- A strong low pressure system passed across the North Sea from west to east, passing Norway, Sweden, the Baltic Sea and the Baltic countries
- A cold air outbreak accompanying the low pressure system
- Open cell structures shown in cloud pictures at 10:00 UTC on 1st November 2011 (see also here Fig. 1)
- High wave field developed first in the northern North Sea and propagated southward along with the strong winds with a long fetch, as shown in wave measurements from offshore buoys
- At FINO 1, a maximum significant wave height H_s of almost 10 m was observed at 04:00 UTC on 1 st November 2011, corresponding to a return period of 20 years.

The simultaneous presence of the open cells and the high waves observed at FINO 1 have triggered continuous interest in the past decade in analyzing and

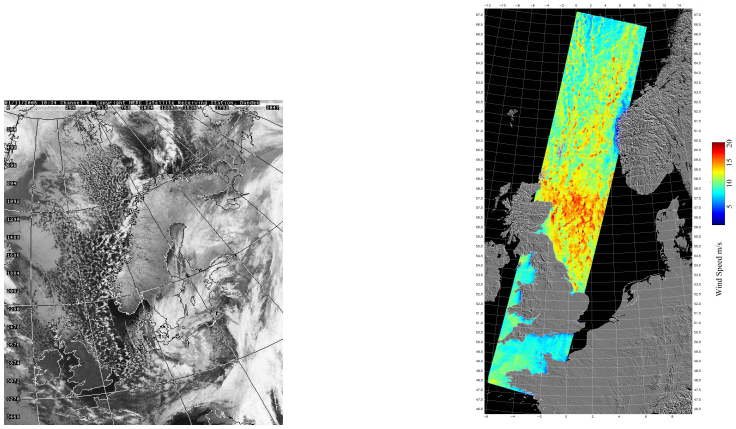

Fig. 1 (a) left: cloud picture, from NOAA 17 satellite, channel 5, on 2006-11-01 10:34 (time of first line: 2006-11-01 10:27:39.359; time of last line: 2006-11-01 10:42:26.097) (b) right: ENVISAT SAR 10 m wind speed on 2006-11-01 10:26:41

modeling the storm Britta, and in interpreting the role of the wind input with organized structures to the wave generation (Brusch et al 2008; Behrens and Günther 2009; Emeis and Türk 2009; Pleskachevsky et al 2012; Kettle 2015b). Open cells, classified as type-I cloud-topped boundary layers by Agee (1987), frequently occur within cold air outbreaks (Atkinson and Zhang 1996). Cold air over warm water surface is modified, leading to formation of clouds which frequently take the form of cloud street, roughly oriented along the winds in the outbreak. Further downwind in the outbreak, the cloud street transforms into three dimensional open cells (Brümmer et al 1992). While moving along with the weather system, in the center of open-cell circulation, there is downward motion and clear sky, which is surrounded by cloud associated with upward motion (Atkinson and Zhang 1996),

see Fig. 1a. Accordingly, there is both spatial and temporal significant fluctuation in the wind field, which will be shown later in our analysis in section 3.1.2. The SAR data transects in Fig. 1b contain fluctuating wind speed at 10 m of about 5 ms^{-1} over 3 km.

To model the atmospheric conditions of storm Britta, Brusch et al (2008) used the non-hydrostatic Local Model nested in Global Model Europe at a spatial resolution of 7 km and a hydrostatic atmospheric model HIRHAM at a spatial resolution of 11 km. Although the 7-km model simulation gave slightly more detailed spatial wind features, neither of the simulations reproduced the open cell structure as shown in the cloud picture. Their spectral analysis of the wind speed time series measured at FINO 1 during Britta showed multiple peaks on the scale of 0.1 to 0.3 hours, which were argued to be equivalent to spatial scales of 30 to 50 km. These scales are of the right order of magnitude when compared to the cell size of cloud patterns.

Emeis and Türk (2009) analyzed the hourly observations at FINO 1 for Britta, together with storm Erwin from 8th January, 2005. The two storms have shown similar wind strength and frictional velocity but H_s is significantly smaller during Erwin (being an 1-3 year event) at the same wind speed than that during Britta (being a 20-year event). Climatological data show that at FINO 1 the largest H_s are accompanied with northerly winds and on average, H_s increases with wind speed most strongly when winds are from the north (e.g. Britta); however it is from the west that the strongest winds are observed (e.g. Erwin). In contrast to the unstable condition during Britta, during Erwin at FINO 1, the air was warmer than water. Stability was considered by Emeis and Türk (2009) as one major cause to the different response of H_s to the wind or stress for the two storms.

Behrens and Günther (2009) modeled Britta using the operational wave forecast system running at the German Weather Service, based on the third generation wave model WAM. The spatial resolution of the wave modeling is about 10 km. The wind input to the wave modeling is the 10 m forecast wind fields delivered by the regional atmosphere model of DWD (Deutscher Wetterdienst) that runs on a grid of about 7 km. Their 3-hourly outputs show that the large values of H_s accompanying the development of the storm are, though slightly underestimated, reasonably well captured by the modeling system for FINO 1. Overestimation by the model was observed at a couple of other sites. The role of the open cells was not mentioned in their study.

The impact of the open cells in accompany with the passing of a cold front, described as the "storm in storm" wind field in Pleskachevsky et al (2012), was examined in their ideal study using the K-spectral model (Schneggenburger et al 2002) with a spatial resolution of 1 km. It is one of the first that systematically examines the impact of open cell structures on the wave generation and propagation. Their study argues that when the atmospheric convection field is travelling near the surface wave speed, a resonance coupling effect is enabled, building up individual rogue wave. Accordingly, an individual-moving open cell can cause the local H_s to increase on the order of meters within the cell area, and that a group of cells produce a local increase in H_s of more than 6 m during 10 to 20 minutes, the time for the cell to pass. In their ideal modeling, the "rapid moving gust structure" was artificially implemented by updating the wind field every 5 min. The gust structure in their study was generated as an idealized hexagon-ring pattern which is superimposed into the existing mean wind field.

To find out the key cause to the development of the extreme H_s observed at FINO 1 is important for modelers to effectively allocate modeling effort to cope with the most relevant issues. The current study aims at shedding more lights into the development of storm Britta through a standard setup of a wind-wave coupled modeling system at high resolution and analysis of various types of measurements. In contrast to previous literature results we here show that the atmospheric open cell structures and the atmospheric stability play a second order role as the recorded large H_s followed the expected wave behavior under the wind and fetch during Britta.

This paper is organized as following: Sec. 2 introduces the various types of measurements, the modeling system and the method for data analysis. Results are presented in Sec. 3, followed by discussion and conclusions in Sec.s 4 and 5, respectively.

2 Method

2.1 Measurements

Wind and wave measurements from 10 stations over the North Sea were analyzed, covering FINO 1 site in the south (54.014°N) and the Norne site in the north (66.0256°N), see Fig. 2 where locations of these sites are marked. Names and coordinates of the 10 sites, period of data and available variables during Britta are listed in Table 1. Apart from FINO 1, the other nine stations are the Norwegian offshore platforms; the data are from www.eklima.met.no and they are 20 min values. It is speculated that the platform construction would cause flow distortion and therefore affect the data quality, particularly at the lower measurement

height such as 10 m. The 10-m wind vectors are studied in relation to the peak wave vectors in section 3. This study is however limited by the direct access to the details of measurement quality from the nine stations and the corresponding analysis regarding the use of these data has been kept qualitative with references to the literatures including Barstow et al (2008), Bitner-Gregersen and Magnusson (2014) and Kettle (2015b). For the presentation of wind time series at Ekofisk, measurements at 116 m were used; the effect of flow distortion should be smaller than the 10-m measurements.

Measurements at FINO 1 are studied in much more details than the other nine stations due to the more complete meteorological and wave dataset. The met mast is instrumented with cup anemometers and vanes at 33 m, 40 m, 50 m, 60 m, 90 m and 100 m for wind speed and directions. Temperatures were measured at 40 m, 70 m and 100 m. Sea surface temperature and water temperatures at 3 m beneath the water surface were measured. The air pressure data are available at 20 m and 90 m. Wave measurements analyzed here were made from a directional waverider DWR (Datawell BV). The data quality was suggested to be good according to the comparison with measurements from four other different instruments where consistent statistics were obtained (Senet et al 2012). At FINO 1, the data are 10 min values for the atmospheric variables and 30 min for the wave variables. In Senet et al (2012), more details about the sea state measurements at FINO 1 can be found.

The satellite cloud pictures (e.g. Figs. 1a and 13) are used to assist the examination of storm development and to identify spatial features in the atmosphere. These pictures are provided by the NERC Satellite Receiving Station, Dundee University, Scotland at http://www.sat.dundee.ac.uk.

Table 1 The sites (sorted from north to south) and their coordinates, measurement periods and variables. U_z is wind speed at height z, WD is the wind direction, H_s is the significant wave height, H_{max} is the maximum wave height, PWD is the wave direction at the peak frequency, T_z is temperature at height z = 40, 70 and 100 m and SST is the sea surface temperature.

site	coordinates	Period	Variables
Norne	8.0850°E, 66.0256°N	2000 - 2012	U_z, WD, H_s, H_{max}, PWD
Heidrun	7.3156°E, 65.3229°N	1996 - 2012	U_z, WD, H_s, H_{max}, PWD
Draugen	7.7792°E, 64.3520°N	2000 - 2012	U_z, WD, H_s, H_{max}, PWD
Ormen-Lange	5.2351°E, 63.5640°N	2008 - 2009, 2011 - 2012	U_z, WD, H_s, H_{max}, PWD
Gullfaks-C	2.2687°E, 61.2042°N	1990 - 2001, 2007 - 2012	U_z, WD, H_s, H_{max}, PWD
Troll-A	3.7193°E, 60.6435°N	2002 - 2012	U_z, WD, H_s, H_{max}, PWD
Heimdal	2.2273°E, 59.5742°N	2003 - 2010, 2012	U_z, WD, H_s, H_{max}, PWD
Sleipner-A	1.9091°E, 58.3711°N	2003 - 2012	U_z, WD, H_s, H_{max}, PWD
Ekofisk	3.2149°E, 56.5453°N	1980 - 1983, 1986 - 2012	U_z, WD, H_s, H_{max}, PWD
FINO 1	6.588°E, 54.014°N	2004 - 2013	U_z, WD, T_z, SST, H_s, PWD

The wind field retrieved from ENVISAT Synthetic Aperture Radar (SAR) during storm Britta is analyzed to complement the in-situ measurements (Fig. 1b). SAR utilizes the fact that radar backscatter from the sea surface depends on centimeter-scale, local wind generated, waves (Valenzuela 1978). The relationship of radar backscatter to the 10-m wind speed is described by an empirical model function (Hersbach et al 2007). The spatial resolution of the SAR data shown as Fig. 1b is about 500 m. The root-mean-square-error of the SAR 10 m wind speed was found to be about 1.3 to 1.5 ms^{-1}, although the bias depends on the model function chosen for SAR wind retrieval (Hasager et al 2011, 2015).

2.2 The modeling system COAWST

This study uses the coupled-ocean-atmosphere-wave-sediment transport modeling system (COAWST) (Warner et al 2010) to reproduce storm Britta. Three model components of COAWST are activated here: the mesoscale atmospheric Weather Research and Forecasting (WRF) model (http://www.wrf-model.org/index.php), the spectral wave model for near shore (SWAN) model (Booij et al 1999) and the Model Coupling Toolkit (MCT).

For modeling the mid-latitude storms using COAWST, through tests on a number of storms with different trajectories, fetches and stability conditions, Du et al (2015) found that the following factors can significantly affect the modeling results regarding the wind and wave characteristics: the model domain position and size, which should be big enough to allow the storm to develop; the spatial resolution, which should be high enough to capture the high temporal and spatial variability of wind during storms; the initial condition regarding the use of large scale data, e.g. Climate Forecast System Reanalysis (CFSR) or Global Forecast System data.

More tests have been done here to storm Britta in order to optimize the setup, regarding the initial time, the simulation period, the spectral nudging technique, the SST data to use and the domain size. It was found that longer simulation period has a higher chance for deviation of the storm development from the large scale forcing and thus the initial time of the storm should not be too early from the storm peak. We tried simulating for 72 hours and observed that the modeling started drifting away from the large scale forcing on day 3. Seemingly, for a fast developing system like Britta, the constrain from the large scale forcing data

becomes important. However, using spectral nudging gave negligible improvement for this case. Second, since the thermal condition is important for the open cells to develop, two types of SST data are examined. It was found through measurements that using the sea surface temperature (SST) from CFSR reanalysis (0.312°) (Saha et al 2010) gives better output of SST at FINO 1 as well as better open cell wind variability than using the NCEP Real-time SST (0.5°). Third, if domain III (Fig. 2) is only half the size of the current setup, the open cells would fail developing. The above arguments are used to guide our model setup described in the following.

The period 2006-10-30 00:00 to 2006-11-02 00:00 was modeled. To obtain a better storm track development, two simulations were performed, each lasting 36 hours. For the two simulations, SWAN is initiated from the default spectrum for the first simulation and the spectrum at the end of the simulation are saved as hot-start files. The hot-start files are then used as the initial spectrum of SWAN for the second simulation. WRF was simply restarted at 2006-10-31 12:00.

The model domain setup is the same for WRF and SWAN, with three nested domains and spatial resolutions of 18 km, 6 km and 2 km for domain I, II and III, respectively, see Fig. 2a and b. For WRF, the domains are two-way nested. There are 46 vertical sigma levels for all WRF domains, with the lowest model level at a height about 10 m. We used MYNN 3.0 PBL scheme (Nakanishi and Niino 2009), Thompson microphysics scheme (Thompson et al 2004) and RRTM long wave and short wave radiation physics schemes (Iacono et al 2008). The Kain-Fritsch cumulus scheme (Kain and Fritsch 1993) is used for domain I, but is deactivated for domain II and III. The Corine land use data are used. The initial and boundary forcing of WRF are the CFSR data. The 0.312° CFSR SST were used.

In SWAN, the 1/8 arc-minute bathymetry data from the Digital Terrain Model (DTM) of European Marine Observation and Data Network (http://www.emodnet-hydrography.eu) was used. The bathymetry is presented in Fig. 2b. SWAN is initiated with a JONSWAP spectrum and the outer domain open boundaries are set to the JONSWAP spectrum with $H_s = 0.5$ m and $T_p = 1$ s, where T_p is the wave period at the spectral peak. We used 36 directional bins and a frequency resolution of $0.1f$ with f the frequency and it is between 0.03 Hz and 1.02 Hz. The wind input and dissipation source functions are based on the studies of Zijlema et al (2012). One-way nesting is used in SWAN.

WRF transfers the 10-m meridional and longitudinal wind components, u_{10} and v_{10}, to SWAN, and SWAN feeds back with the wave period at the spectral peak, which is used to calculate the wave age (c_p/u_*, with c_p the wave phase velocity at the peak frequency) and thereafter roughness length (z_0). Here, the roughness length z_0 is calculated through the Fan et al (2012) algorithms:

$$z_0 = \alpha u_*^2/g + 0.11\nu/u_* \tag{1}$$

where ν is the viscosity coefficient, g is the gravitational acceleration and α is the Charnock parameter which is parameterized with the wave age c_p/u_*:

$$\alpha = a(c_p/u_*)^{-b} \tag{2}$$

with

$$a = \frac{0.023}{1.0568^{U_{10}}}, \quad b = 0.012U_{10} \tag{3}$$

where U_{10} is the wind speed at 10 m and $U_{10} = \sqrt{u_{10}^2 + v_{10}^2}$. The Fan algorithms are not included in the original COAWST but implemented here. Our

earlier studies, Bolaños et al (2014) and Du et al (2015), show that the Fan algorithms give reasonable roughness length in comparison with measurements. Data are exchanged every 90 seconds between WRF and SWAN through MCT.

The atmospheric model WRF can be used together with the wave model SWAN in various ways. One often-used approach is the so-called one-way offline coupling, meaning that the wind field from WRF is used as input to force SWAN, but SWAN does not feedback to WRF with any wave information. This approach is also tested here in our process of optimizing the model system setup, where the default WRF description of the roughness length is used. In this description, the roughness length z_0 follows Eq. 1, whereas the Charnock parameter α is a linear function of wind speed at 10 m. The online coupling outperforms the offline coupling both in the wind and significant wave at FINO 1, particularly the magnitude and wind speed and H_s at the storm peak. The offline coupled modeling gives underestimation of the wind speed at storm peak by 2 ms^{-1} and H_s at storm peak by 1 m. However, the focus of the current study is to examine the effects of the open cell structures and stability related to the wind field in finding out the necessary conditions for the extreme H_s observed in the southern North Sea, we go on with the satisfactory approach of using online coupling and do not go into details of the effect of coupling.

2.3 Method for data analysis

COAWST, together with various types of measurements over the North Sea (see Sec. 2.1), are used jointly to study the development of storm Britta.

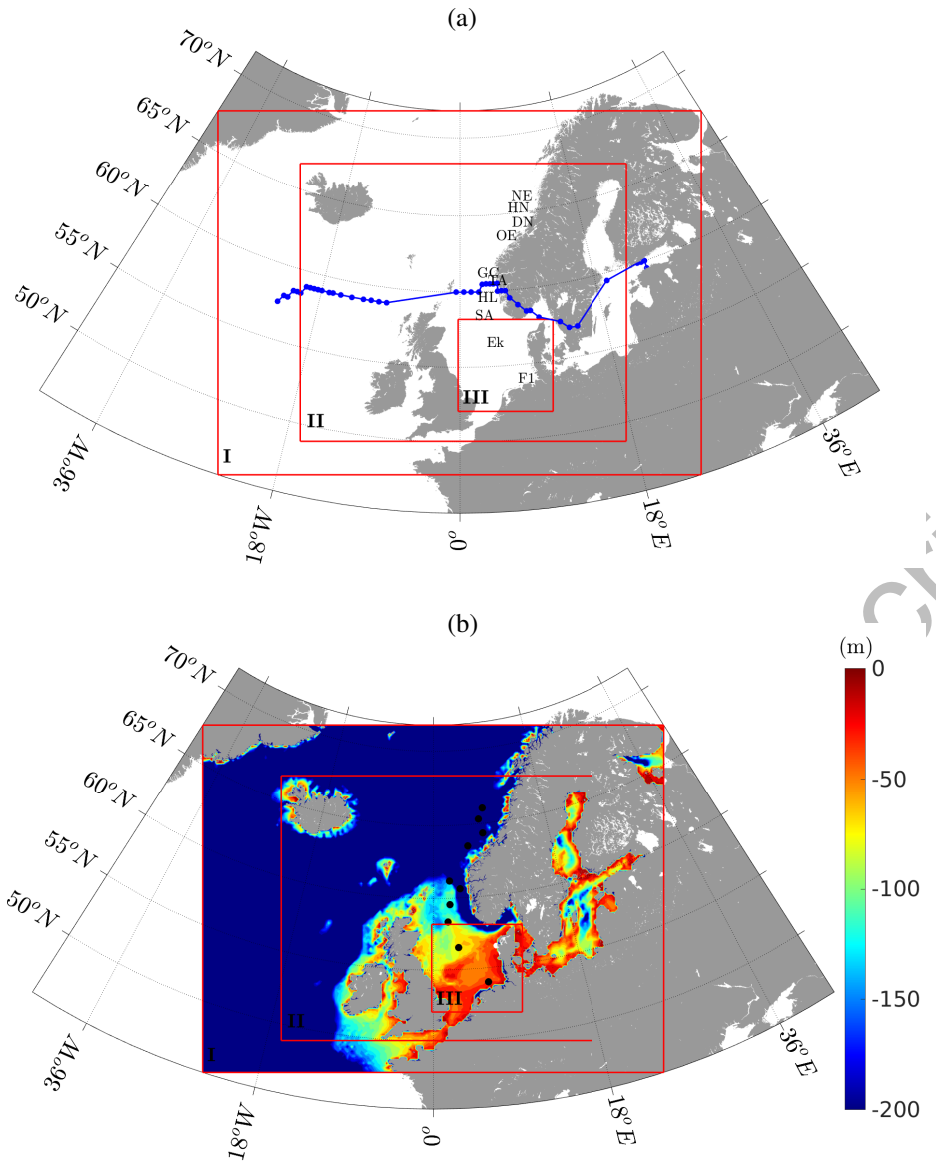

Fig. 2 (a) The three nested model domains of WRF and SWAN, domain-I, II and III for the outermost, middle and innermost domains, with resolutions of 18 km, 6 km and 2 km, respectively. Also shown are the 10 measurement stations, marked by the first and last letter of their names as given in Table 1. The blue dots linked by a line show the storm center of Britta during 2006-10-30 00:00 to 2006-11-01 05:00. (b) Bathymetry over the three model domains and the black dots show the positions of the 10 stations as in (a).

To help understanding the role of open cells on the generation of waves, another storm was selected due to the presence of the open cell structure but the absence of extreme H_s. During this storm, winds peaked on 2011-12-13 at FINO 1; we address it herein as the 2011-Dec storm. The wind and wave conditions during Britta and the 2011-Dec storm will be analyzed in the same manner through simultaneous measurements from the 10 stations over the North Sea.

The choice of the 2011-Dec storm also favors the analysis of the stability effect since it resembles storm Erwin from the study of Emeis and Türk (2009) in several ways, including the storm path, the distribution of H_s with wind speed, the wind strength and the wave height. The main difference between them is that at FINO 1, it is stable conditions during Erwin but unstable during the 2011-Dec storm (Table 2).

To further assist the investigation of the physics and mechanisms of the Britta wind-wave relation, additional 10 storms are identified from years of measurements from FINO 1 (2005 - 2013) where the following conditions are satisfied: wind speed at 33 m $U_{33} > 10$ ms^{-1} and $H_s > 6$ m. In connection with the data availability at FINO 1, storms mentioned in Emeis and Türk (2009) and Behrens and Günther (2009) from year 2005 were also analyzed. These storms are listed in Table 2, where the dates of the storm peaks are given, as well as the comparison of the temperature at 40 m (T_{40m}) and SST which indicate approximately the atmospheric stability conditions: unstable with $T_{40m} < SST$, neutral with $T_{40m} \approx SST$ and stable with $T40m > SST$.

Here we consider the significance of the following points in the development of storm Britta:

Table 2 The list of storms sorted according to time: the maximum significant wave height H_s from buoy measurements and an average air and sea surface temperature comparison (T_{40m} versus SST) at FINO 1. "-" means either the atmospheric temperature or SST, or both, is missing. *: 20071109 wave data from AWAC. Britta and the 2011-Dec storms are highlighted with Bold face. Storms with names are listed in Emeis and Türk (2009) and Behrens and Günther (2009)

date	max H_s (m)	temperature	storm name
20050108	6.3	$T_{40m} > SST$	Erwin
20061101	9.8	$T_{40m} < SST$	Britta
20061112	6.2	$T_{40m} < SST$	
20061231	4.3	$T_{40m} \approx SST$	Karla
20070118	5.5	$T_{40m} \approx SST$	Kyrill
20071109	10.1*	-	Tilo
20080127	4.8	-	Paula
20080301	7.3	-	Emma
20101112	7.3	$T_{40m} \gtrsim SST$	
20111207	7.6	$T_{40m} < SST$	
20111213	4.9	$T_{40m} < SST$	"The 2011-Dec storm"
20111229	6.1	$T_{40m} \approx SST$	
20120105	7.6	$T_{40m} \approx SST$	
20120113	6.1	$T_{40m} \lesssim SST$	
20120831	6.6	$T_{40m} < SST$	
20121125	7.1	$T_{40m} \approx SST$	
20130130	6.4	-	

1. The fetch.
2. The atmospheric stability, as addressed by Emeis and Türk (2009).
3. The presence or absence of the open cells, as addressed by several studies.
4. The presence or absence of H_s (return period T larger than 10 years).

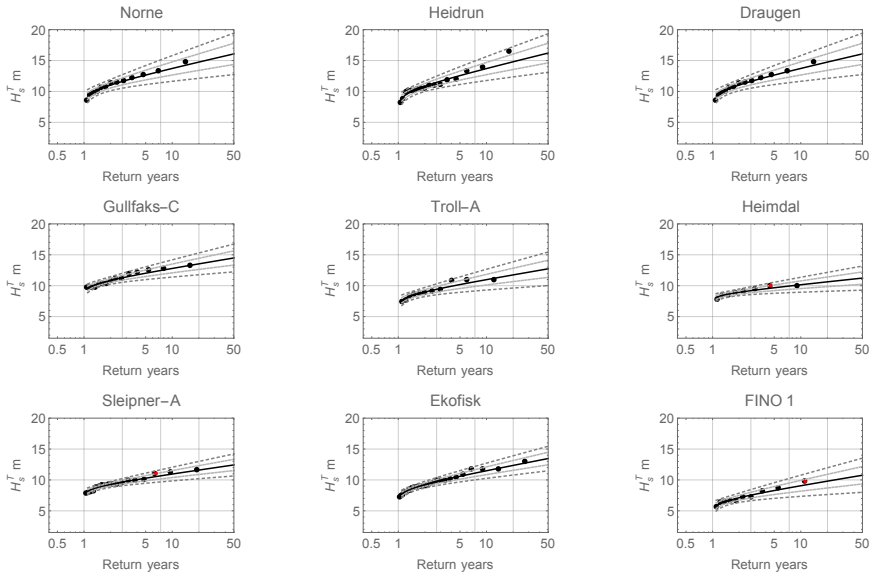

Fig. 3 Distribution of the annual maximum significant wave height H_s at 9 stations, with measurements from buoys. The black solid curves are the Gumbel fit to the samples and the dashed curves are $H_s^T \pm 1.96 \cdot \sigma(H_s^T)$ showing the 95% confidence interval (outside) and $H_s^T \pm \sigma(H_s^T)$ (inside). H_s from storm Britta are among the annual maximum samples at Heimdal, Sleipner-A and FINO 1 and they are marked with a red dot in the corresponding panel. At Ekofisk the maximum H_s was not recorded. At the other sites, H_s during Britta were not large enough to be the annual maximum values.

This return period of a certain H_s is calculated from a Gumbel distribution fit applied to the annual maximum values. Figure 3 shows the Gumbel distribution of the annual maximum H_s for 9 stations where the data length is 8 years or longer; see details of the applied data in Table 1. The site Ormen-Lange station was not included because the dataset is too short. The algorithms for calculating the Gumbel distribution are given here briefly in the Appendix. Thus, the significant waves at FINO 1 and Ekofisk during Britta correspond to a return period of 20 years (cf. Figure 3 regarding the Gumbel fitting and Table 3).

3 Results

The results are presented in two parts. The first part, Sec. 3.1, shows the development of storm Britta through measurements (cloud picture, SAR image, wind and wave measurements from stations) and modeling. The second part, Sec. 3.2, shows the analysis of a number of other storms, including the 2011-Dec storm, through measurements over the North Sea. In order to find out what distinguishes Britta from these storms, the additional storms mentioned in the literature and ten more identified from the FINO 1 measurements (Table 2) were also analyzed.

3.1 Britta

The analysis of Britta is presented in two parts: the storm development (Sec. 3.1.1), and the characteristics of the organized mesoscale feature open cell and its impact on a series of model parameters (Sec. 3.1.2).

3.1.1 Development of storm Britta

The storm path of Britta is shown in Fig. 2a in linked blue dots, from west to east. These dots are positions of the minimum mean sea level pressure (MSLP) identified from the hourly CFSR data from 2006-10-30 00:00 to 2006-11-01 05:00. Note that the low MSLP may cover a relatively large area (see e.g. Fig. 5) and there are sometimes two storm centers (see e.g. Fig. 5 2006-10-31 12:00), so that the storm centers identified through the lowest value of MSLP are rather approximate. For instance, the long distance jump of the storm center position as shown in Fig. 2a is caused by the formation of a new lowest MSLP, which can vaguely be seen in Fig. 5 2006-10-31 06:00. A series of cloud pictures are available from the Dundee

website for the studied period 2006-10-31 to 2006-11-01, showing the center of the visual cloud vortex passing from Northern UK to Norway, again passing Katgat over Southern Sweden and over to the Baltic Sea, in consistency with the blue dots in Fig. 2a. From the cloud pictures, it can be observed that mesoscale features of rolls and open cells developed as the cold front passed by, following the description in Atkinson and Zhang (1996). The area covered by the open cells expanded and Fig. 1a shows the cloud picture at 10:34 am on 2006-11-01, where it can be seen that the Northern Atlantic and the North Sea were covered by open cells. By 22:04 on 2006-11-01 (not shown), it can be read from the cloud picture that open cells are evenly distributed over the whole water body of the North Sea, except for the Katgat. These conditions stayed until mid-morning of 2006-11-02 when the open cells started to dissolve in the northern part of the North Sea, as a result of the development of another storm from the west, when the thermal structure over the North Sea changed. Open cells with diameters of about kilometers to tens of kilometers are not expected to be resolved in a typical QuikScat data which are of a resolution of 25 km (Brusch et al 2008). Here the snapshot of SAR data at 2006-11-01 10:26:41 am, with a spatial resolution of about 500 m, shows clearly the presence of these mesoscale features over a band covering part of the North Sea, consistent with the cloud picture (Fig. 1).

The development of the storm is also examined with available measurements from the 10 stations. Figure 4 shows the wind vectors (red arrows) and peak frequency wave vectors (blue arrows) from 06:00 on 2006-10-31 to 16:00 on 2006-11-01. One can see that at 06:00 on 2006-10-31, the winds at the southern stations were from southwest and so were the waves from some of these stations; at the northern stations, the winds were from northeast and the waves were propagating

from north to south. As the storm center moved southeasterly, the mean winds turned gradually toward the south and the wave field adjusted accordingly and by the end of 2006-10-31, the winds and waves are almost aligning with each other again, with winds at the middle stations becoming the strongest. The strongest winds continued moving to the south and FINO 1 experienced its maximum wind speed and wave height at about 04:00 on 2006-11-01, as can be seen from the time series shown in Fig. 6. To help understanding the wind field, the isobars are shown in Fig. 5 for the same time of the subplots of Fig. 4. Here one can see that the south-north oriented isobars are persistent for many hours, favoring the southerly winds.

The model captured these observed wind and wave features of the storm. The spatial distribution of temperature and SST from modeling show that, at the initial stage of Britta, cold air advected from the north to the south, and the air and water temperature difference at FINO 1 reached about -7° at 04:00 on 2006-11-01 ($OBS\ SST - T_{40m}$ or $MODEL\ SST - T_{2m}$, Fig. 6). Under this unstable condition, open cell structure in the wind field developed and the area covered with such structure became larger, extending to the southern part of the North Sea. Figure 7 shows four snapshots of modeled U_{10} over model domain III. Figure 7a corresponds to the time when the storm winds at FINO 1 peaked; the modeled U_{10} reached about 24 ms^{-1} around FINO 1 and there is a high spatial variability in U_{10}. Figure 7b is when both cloud picture and SAR data are available (Fig. 1). At this time, the modeled open cells cover half of the North Sea, in agreement with the cloud picture and SAR image. Fig. 7c (13:00) and d (22:00) are included to show further development of open cells over the space. By 22:00, most of domain III is covered by evenly distributed open cells (Fig. 7d), which is also consistent

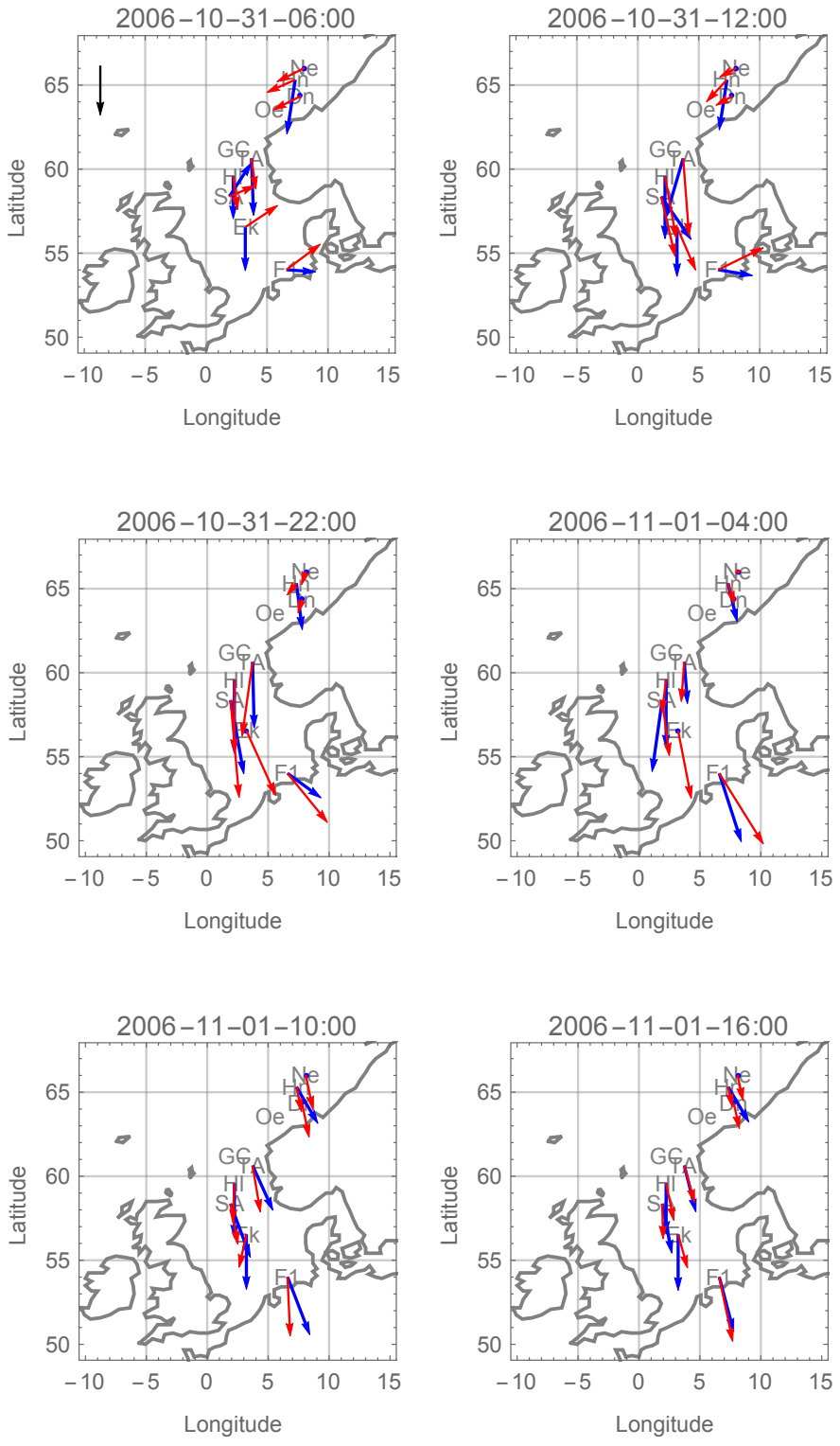

Fig. 4 Wind vectors (red arrow) and wave vectors (wave velocity and direction at the peak frequency, blue arrows) at stations where data are available during storm Britta. At FINO 1, the wind speed at 100 m and direction at 90 m were used; at other sites, winds from 10 m are used as obtained by the data provider. The time is printed in the figure labels. The arrow at the upperleft corner in the first sub-plot shows a direction from the north with a magnitude of 20 ms^{-1}, which applies for both wind and wave.

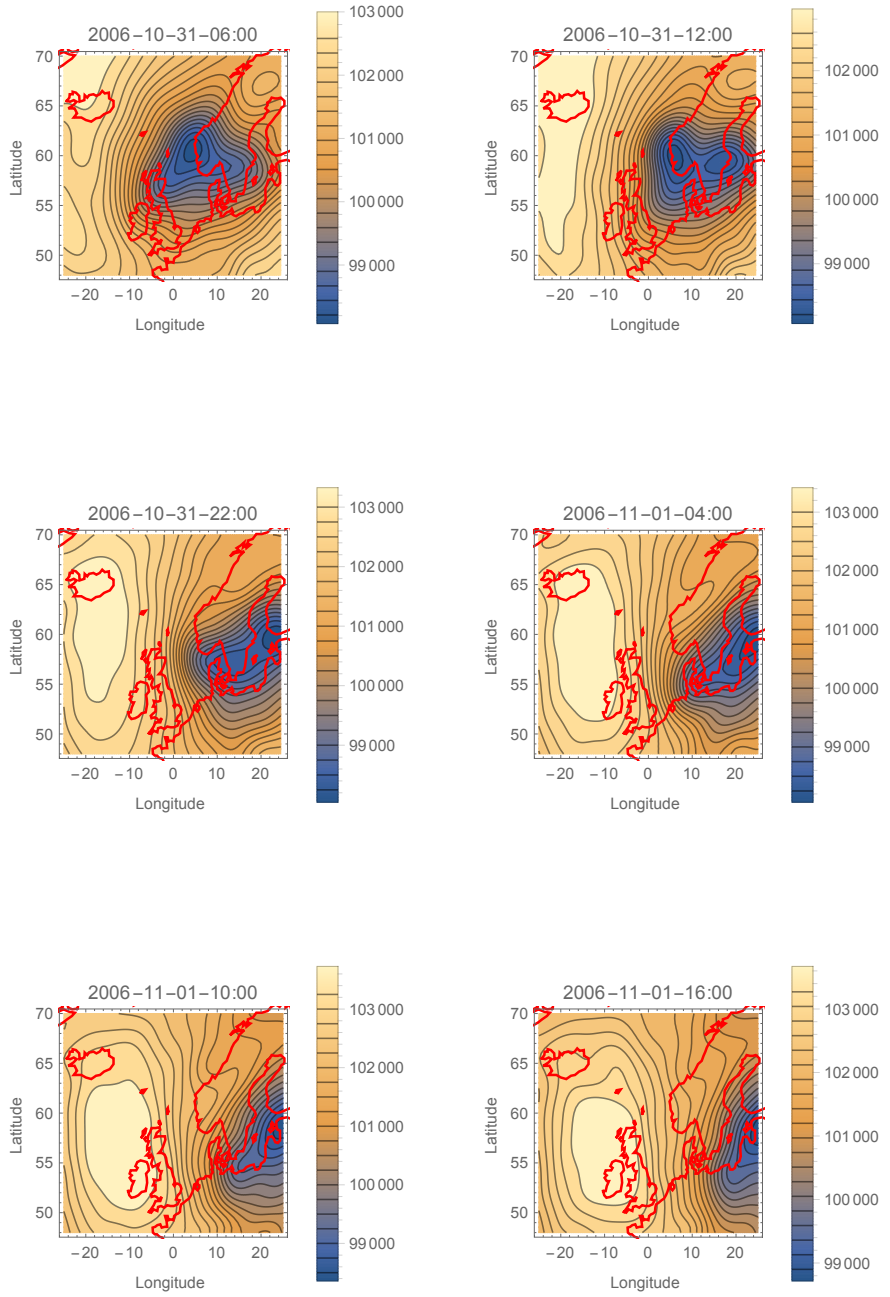

Fig. 5 Isobars during storm Britta, at corresponding time to Fig.4.

with cloud pictures (not shown). Note that, the color scale differs in the subplots and the intention is to enhance the organized structures in the wind field.

In Fig. 6, modeled and measured variables at FINO 1 are shown. Here the modeling results are all from domain III. The modeled pressure is in phase with the measurement and it captured the lowest values. The modeled MSLP was corrected to the measurement height of 20 m by using a lapse rate of 0.0065°C per meter. The various temperatures are displayed to show the variation of atmospheric stability with time. The modeled atmospheric temperatures at 2 m has not been converted to the measurement height of 40 m due to the lack of a reliable temperature profile model. However, using the same lapse rate as used for pressure gives a decrease of about 0.2 °C from 2 m to 40 m, which is small. The modeled and measured SST are in perfect agreement. Both the modeled wind speed and H_s follow the measured values and the peak values during the storm are rather well captured. Though we note that our calculation gives the peak one hour too early. Similar performance is found at Ekofisk (also inside domain III, see Fig. 2a) during initial growth and final decay of the storm. According to Kettle (2015b), during Britta, Ekofisk recorded the largest H_s among the nine Norwegian platforms, and one of the three independent wave measuring systems on the Ekofisk production complex showed maximum wave height reaching 22 m above mean sea level. Kettle (2015b) also commented that the sensors indicated quality issues. The measurement dataset to which the current study had access misses a few values of H_s at the storm peak, see Fig. 8; and pressure and temperature measurements are not available at Ekofisk. Note that there seems to be more fluctuation in the modeled wind speeds than in the measured ones. This could partly be caused by the fact that the modeled

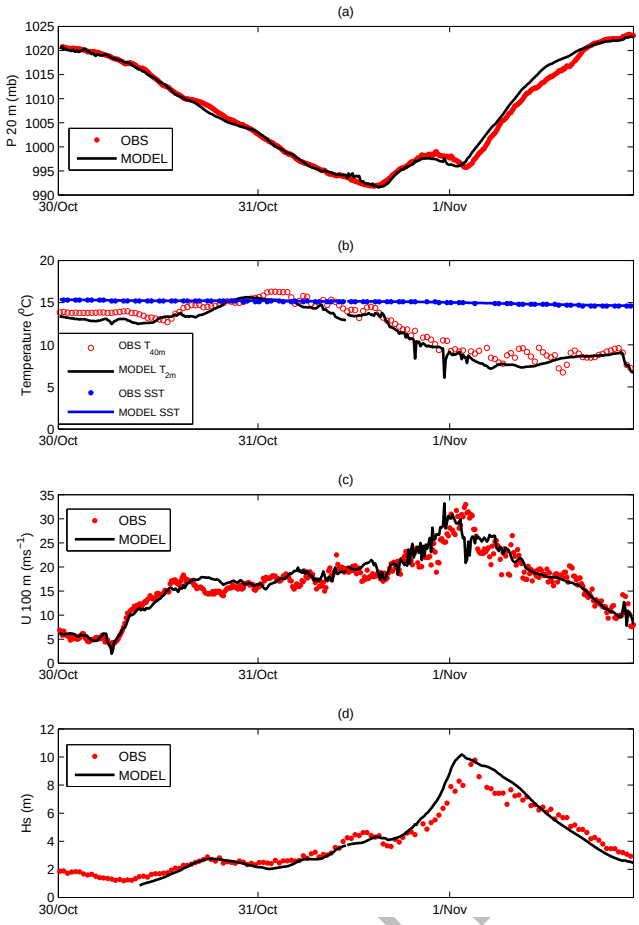

Fig. 6 At FINO 1, time series of pressure at 20 m (a), temperatures (b), wind speed at 100 m (c) and significant wave height (d), measured and modeled. x-axes shows the day

time series are 10-min disjunctive values while the measured time series are 20-min mean values.

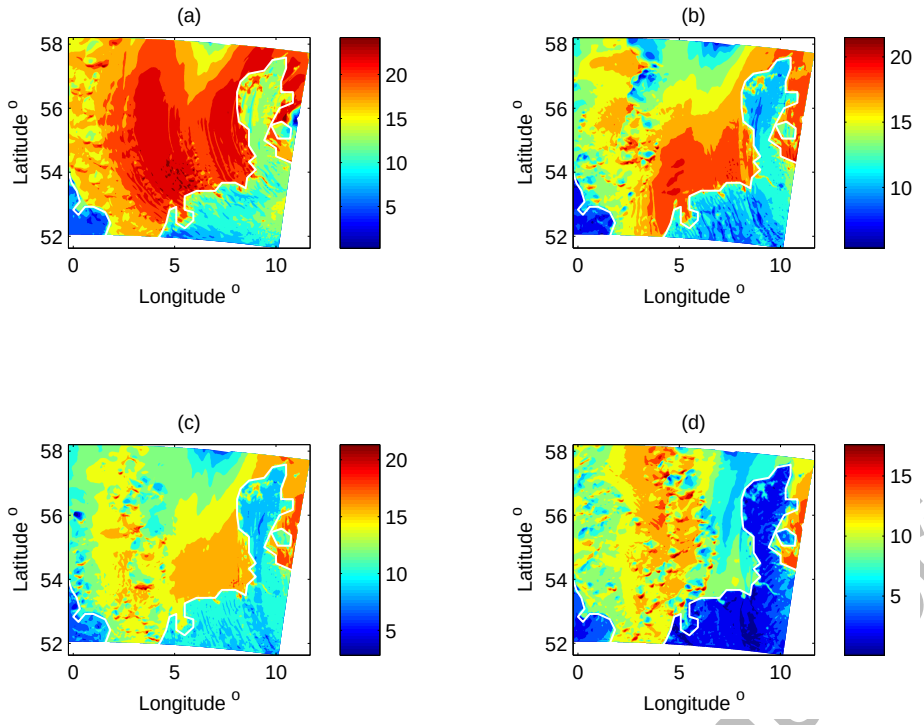

Fig. 7 Modeled wind speed at 10 m on 2006-11-01, at (a) 04:00 (b) 10:00 (c) 13:00 (d) 22:00, domain III. The color bars are in ms^{-1}.

3.1.2 Open cells: characteristics and impact

The open cells are characterized by highly fluctuating wind speed, not only spatially (Fig. 1b), but also temporally within the time frame of approximately a few hours.

The power spectrum of wind speeds related to open cells is characteristic of active energy within a certain temporal and spatial scale. This scale distinguishes the open cell wind spectrum from normal storm spectra. The exact scale though depends on the size of the open cells. The significantly higher spectral power due to open cells than the climatological values have been reported in Larsén

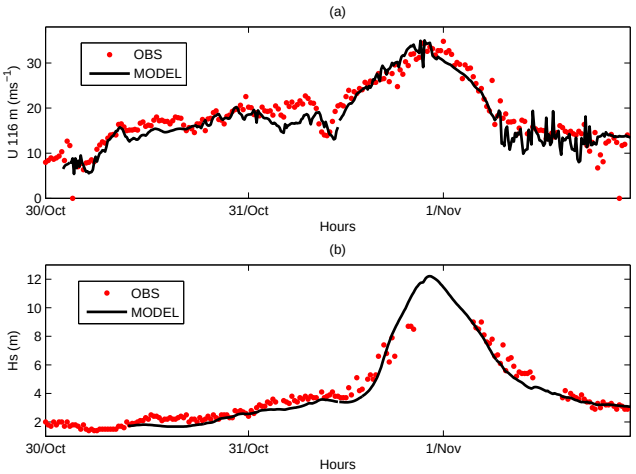

Fig. 8 At Ekofisk, wind speed at 116 m (a) and significant wave height (b), measured and modeled. x-axes shows the day

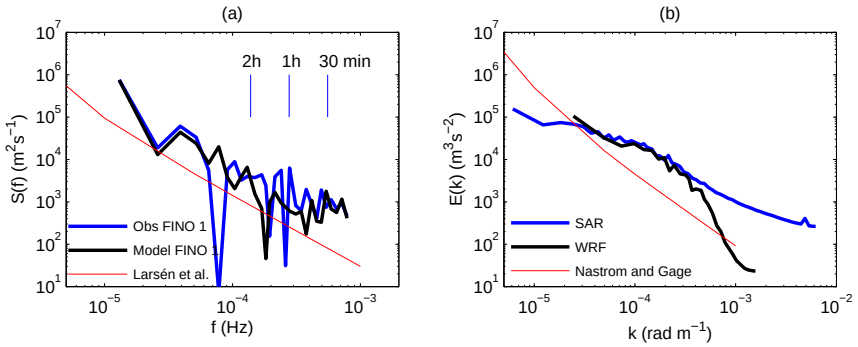

Fig. 9 (a) At FINO 1, power spectra as a function of frequency f from time series between 2006-10-31 16:00 to 2006-11-02 00:00. The blue curve is from measurements of wind speed at 100 m and the black curve is from modeled time series of wind speed at 100 m. The red curve is the spectral model from Larsén et al (2013). (b) Power spectra as a function of wave number k from snapshots of the 10 m wind speed, the blue curve is from the SAR 10 m wind speed as in Fig. 1 and the black curve is from the modeled 10 m wind from domain III as in Fig. 7b the left half part. The red curve is the k-spectrum from Nastrom and Gage (1985).

et al (2013) with their 10-min wind speed time series (for the frequency range $6 \cdot 10^{-5} - 10^{-3}$ Hz) and in Larsén et al (2016) with sonic 20 Hz time series (for the frequency range $6 \cdot 10^{-5} - 10^{-2}$ Hz). Brusch et al (2008) analyzed power spectrum of the two-day 10-min wind speed time series from FINO 1, from October 31 to November 1, 2006, as a function of period, and they observed multi-peaks in time scales from 0.1 to 1.0 hour. The power spectrum of the time series of the wind speed at 100 m from 4 pm on October 31 to 00:00 November 2, 2006 was also calculated and presented here in the frequency domain in Fig. 9a. Time scales of 30 minutes, 1 hour and 2 hours are indicated with the vertical lines. Here the blue curve (U_{100} at FINO 1 from Britta) is above the red curve (climatological data from Larsén et al (2013)), indicating more wind fluctuations. Consistent with Brusch et al (2008)'s analysis, there are multiple peaks in the power spectrum in their time scale range of less than 1 hour. Note that the time series is rather short for a Fourier Transformation and the uncertainty related to the individual spectral peaks is considerable. Correspondingly, in Fig. 9b, the power spectrum of the SAR winds from Fig. 1b as a function of wave number k shows higher values for $k > 5 \cdot 10^{-5}$ rad m^{-1} than those for normal wind conditions (Nastrom and Gage 1985; Gage and Nastrom 1986). Note that here all SAR data north of the northern UK coastline are used for the spectral analysis; the data size is $N \times 758$, where N is the number of pixels from the northern boundary of the SAR image to the coastline of UK in the north and N ranges from 1038 to 3246. The spectrum from each transect ($N \times 758$) is first calculated and averaged afterwards for each frequency and shown as the blue curve in Fig. 9b. The absolute value of the SAR wind is known to be uncertain when U_{10} is greater than about 20 ms^{-1}. However, the spatial distribution of the mesoscale SAR wind features being very similar to

the cloud picture (Fig. 1a and b) is useful for providing a qualitative picture of the spatial wind variation.

The corresponding COAWST modeled wind field in Fig. 7b shows similar spatial features to Fig. 1b. The wave number spectrum $E(k)$, calculated with 10-m winds from the west half part of domain III from Fig. 7b (in order to overlap with the SAR data), agrees well with measurements for $k < 3 \cdot 10^{-4}$ rad m^{-1}, but the energy level dropped rapidly for smaller scales. This is a known fact for mesoscale numerical modeling, such as WRF, that the wind variations in the mesoscale range are smeared because of averaging effects embedded in the modeling (Skamarock 2004; Frehlich and Sharman 2008; Larsén et al 2012). For WRF, an effective resolution is approximately 7 times the model spatial resolution (Skamarock 2004). The comparison shown in Fig. 9b suggests that the spatial wind variation within the scale of about 15 km with the WRF output is, as expected, smaller than what measurements or theory would give. In the temporal domain, from Fig. 9a, it can be seen that the modeled time series slightly underestimates the wind variation, and the frequencies and the magnitude of the multiple spectral peaks are not exactly the same. From the SAR image it can be observed that there is a range of sizes of open cells, which explains the multiple peaks. Seemingly the model did not reproduce exactly the same sizes of open cells. However, the general level of energy and the presence of the multiple peaks in the relevant frequency ranges are in good agreement between the modeled and measured data up to 10 min resolution.

The spatial structure of the open cells is present in a number of WRF variables, such as the momentum flux, sensible heat flux and roughness length, whose calculations are involved with the wind speed. To examine how the spatial structure of the open cells in the wind field affects the calculation of wave parameters, we

examined at each model time step the action density ocean wave spectrum and each term in the source function

$$S_{tot} = S_{in} + S_{ds} + S_{nl} \quad (4)$$

where S_{tot} is the source function, which is superposed of source terms due to wind input, S_{in}, dissipation due to white capping, bottom friction and depth-induced wave breaking S_{ds} and non-linear wave-wave interaction S_{nl}. Figures 10 and 11 show snapshots of S_{in}, S_{ds} and S_{tot} in Eq. 4 at 04:00 and 22:00 on 2006-11-01, respectively. Figure 10 corresponds to the storm peak at FINO 1 when open cells are mostly over the western part of the North Sea; Fig. 11 is chosen because open cells are covering most of the water. S_{nl} values are about zeros and they are not shown. Similar patterns of open cells as in the wind field are present in S_{in}, S_{ds} and in S_{tot}. However, the average magnitudes of these terms differ. S_{in} and S_{ds} are on the same order, with $S_{nl} \sim 0$, leaving the sum of them, S_{tot}, about six and five times smaller than the magnitude of S_{in} for Fig. 10 and Fig. 11, respectively, see the legends. Even though the impact of the modeled open cell wind field is still present on the calculation of H_s through the wave spectrum, the change of the spectrum from this impact is much smaller than the mean value of H_s in general (about 1%). Accordingly, there is no obvious open cell feature in the spatial distribution of H_s; Fig. 12 shows the corresponding H_s fields from domain III to the wind fields shown in Fig. 7.

The standard way of calculating the atmospheric stress is based on stationary boundary layer turbulence statistics which assumes almost zero energy in the range $f < 10^{-3}$ Hz. This is also the case in the WRF modeling. This assumption is invalid in the presence of the open cells, as suggested by Fig. 9 as well as in the studies

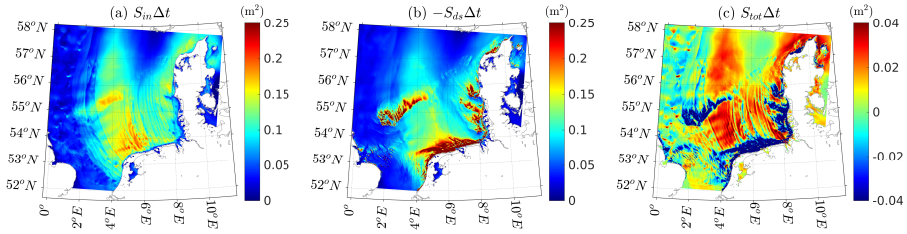

Fig. 10 Snapshots of source terms at one time step $\Delta t = 90$ s (WRF-SWAN data exchange rate) at 04:00 on 2006-11-01, (a) S_{in} wind input (b) S_{ds} dissipation due to whitecapping, bottom friction and depth-induced wave breaking (c) S_{tot} the total wave energy.

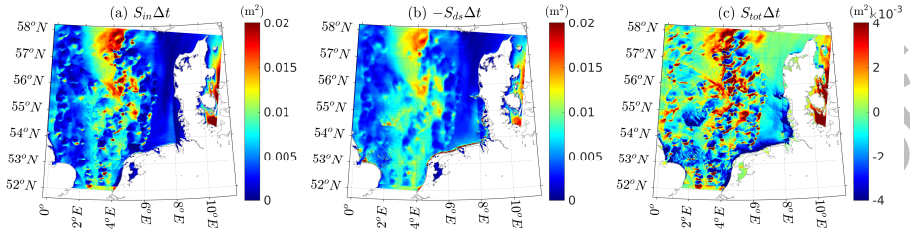

Fig. 11 Same as Fig. 10, except for 22:00 on 2006-11-01.

of Larsén et al (2013, 2016). In the current modeling, the open cell wind field is brought to the wave modeling through the spatial distribution of the WRF wind. The extraordinary energy from the open cells shown in the power spectrum from measured 10-min wind time series is not included in the calculation of the exchange between wind and wave fields as described in the current modeling system.

3.2 The 2011-Dec storm and other storms in the North Sea

The maximum values of H_s during Britta and the 2011-Dec storm at the 10 stations are listed in Table 3, together with their return period T and the maximum wind speed during the two storms. The return period for H_s was calculated from

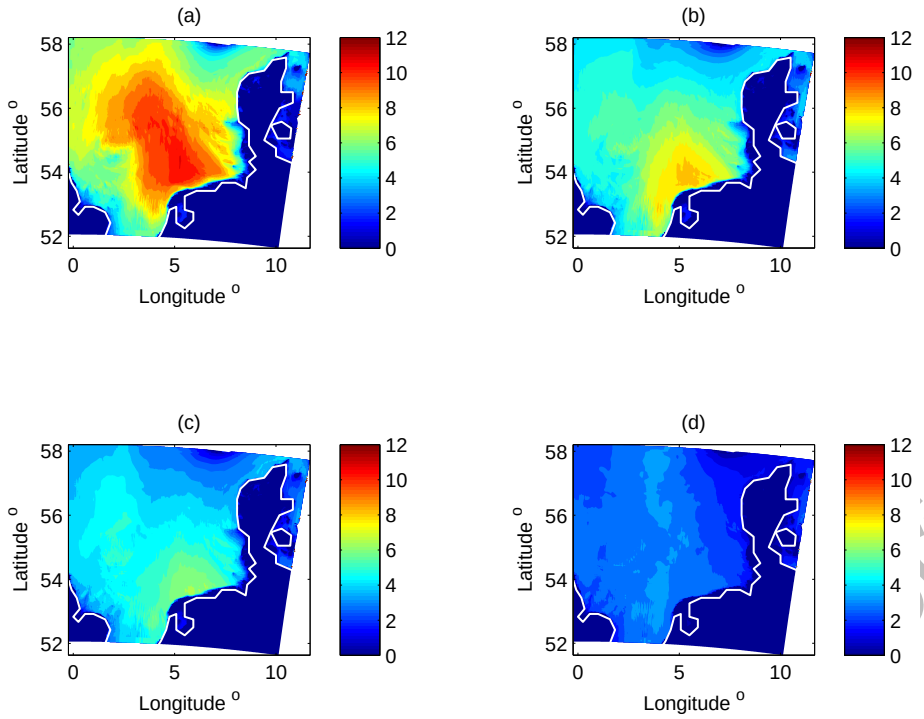

Fig. 12 Modeled significant wave height on 2006-11-01, at the same times as Fig. 7: (a) 04:00 (b) 10:00 (c) 13:00 (d) 22:00, domain III.

the Gumbel distribution of the annual maximum H_s at these stations as shown in Fig. 3. T has been rounded to the closest integer.

The numbers in Table 3 suggest that H_s during Britta can be classified as extreme value at FINO 1 and Ekofisk, with both being a once in 20-year event, and possibly also at Sleipner-A and Heimdal, both being an once in 8-year event, but at the other stations H_s are within 1 year return period.

The 2011-Dec storm did not create extreme H_s at these stations, even though there are several facts that are similar between this storm and storm Britta: cold fronts accompanied with open cells development over the North Sea under convective conditions and strong winds. The cloud picture, Fig. 13, shows the weather

Table 3 Maximum value of H_s during Britta and the 2011-Dec storm and their return period T (rounded to the integer) and the maximum wind speed U during the storm. The wind speeds U at all sites are at 10 m, except for FINO 1 where it is at 33 m (in italic). "-" means missing data. "—" means the data record is too short (less than 2 complete years) to make a Gumbel distribution. *Ekofisk data missing at the peak of the storm, 12.2 m is from the wave modeling (see Fig. 8). ⋆: 9.4 m from AWAC and 9.8 m from Buoy.

site	Britta			2011-Dec		
	H_s (m)	T (yr)	U (ms^{-1})	H_s (m)	T (yr)	U ms^{-1}
Norne	5.2	1	14	5.2	1	22
Heidrun	4.3	1	12	4.6	1	19
Draugen	5.2	1	14	5.2	1	22
Ormen-Lange	-	-	-	5	–	
Gullfaks-C	-	-	-	-		
Troll-A	8.1	1	28	7.9	1	24
Heimdal	10.0	8	25	-	-	
Sleipner-A	11.0	8	29	8.8	2	23
Ekofisk	12.2*	20	25	10	3	24
FINO 1 ⋆	9.8 (9.4)	20	*27*	4.9 (4.3)	1	*23*

system at 2011-12-13 13:23, where the open cell structure is visible over the North Sea. SAR data are not available for this case. During this storm, waves at Ekofisk are most rarely high compared to other sites, and they have a return period of only 3 years. Therefore the open cell structures are not the main reason of the development of extreme H_s.

During the development of the open cells, at FINO 1, the temperature difference between atmosphere at about 40 m and water surface was -5 ° at 2011-12-12 00:00 and increased to -1 ° at 2011-12-14 00:00. It is unstable stratification, like Britta, except that Britta had greater temperature difference. In the scatter plot of

H_s with U_{100} for data at FINO 1, H_s is smaller at the same U_{100} for the 2011-Dec storm than that for Britta, similar to what was found for storm Erwin in Emeis and Türk (2009). Recall that during storm Erwin, at FINO 1, the atmosphere is warmer than the water surface; this factor was argued to be a possible cause to the difference in the $H_s - U_{100}$ distribution from Britta. The 2011-Dec storm does therefore not support that argument. We note also that the CFSR MSLP also shows similar trajectory of the storm center (lowest MSLP) over the North Sea for the 2011-Dec storm and storm Erwin.

Together with a series of the cloud pictures from 2011-12-12 on, the analysis of the CFSR reanalysis MSLP data and the wind and wave measurements from the stations tells that the cold front passed the Atlantic Ocean north of UK and continued northeasterly and northward. The evolution of the wind and peak wave at the 10 stations can be seen in Fig. 14, which follows well the isobars shown in Fig. 15. The wind has been turning from one direction to another (red arrows in Fig. 14).

Referring to the four conditions as listed in section 2.3, both the 2011-Dec storm and Britta are of unstable conditions and both have open cells present. However, during 2011-Dec storm, the stations are exposed to a fast changing wave fields and when the waves are from the south, or southwest, the fetch is much shorter than that during Britta.

Both the 2011-Dec storm and storm Erwin have similar magnitude of H_s at the same wind speed and none has extreme H_s developed at FINO 1. Moreover, both have interrupt fetches for wind and wave during short periods. However, the 2011-Dec storm has unstable atmospheric stratification and open cells are present, and Erwin has stable stratification and open cells are absent.

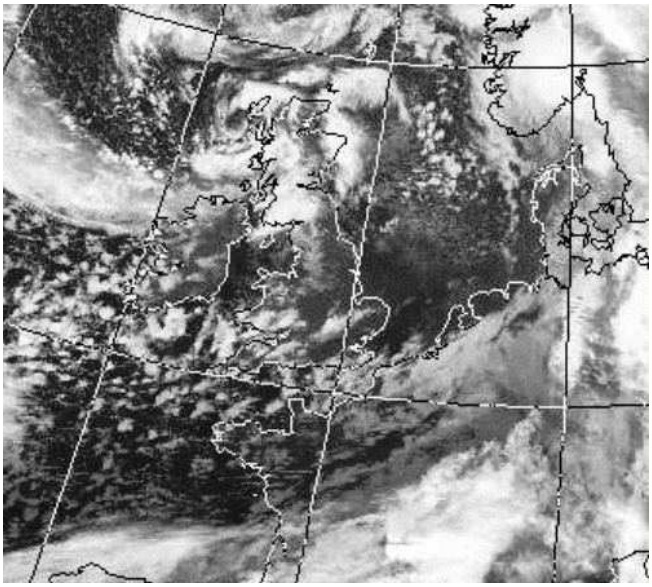

Fig. 13 Could picture on 2011-12-13 13:23, obtained from *http://www.sat.dundee.ac.uk/abin/browse/avhrr/*2011/12/13

In the storm list in Table 2, one storm is particularly worth mentioning, namely, storm Tilo, which was also mentioned in Emeis and Türk (2009) and listed in Behrens and Günther (2009). During storm Tilo, AWAC at FINO 1 measured the peak $H_s = 10.1$ m on 2007-11-09, which is yet another 20-year return value. The interesting observations are that, firstly, the storm path, defined according to the lowest MSLP from CFSR data, from afternoon 2007-11-08 on, is rather similar to that of Britta. The CFSR MSLP shows a spatial distribution of the isobars with an orientation from north-northwest to south-southeast over the North Sea for days, allowing the waves grow high along with the strong and undisturbed wind field. Secondly, the wind and wave measurements are available at five sites, Heidrun, Draugen, Gullfaks-C, Sleipner and Ekofisk and they show that the wind and peak wave vectors are persistently pointing from north-northwest to south-southeast

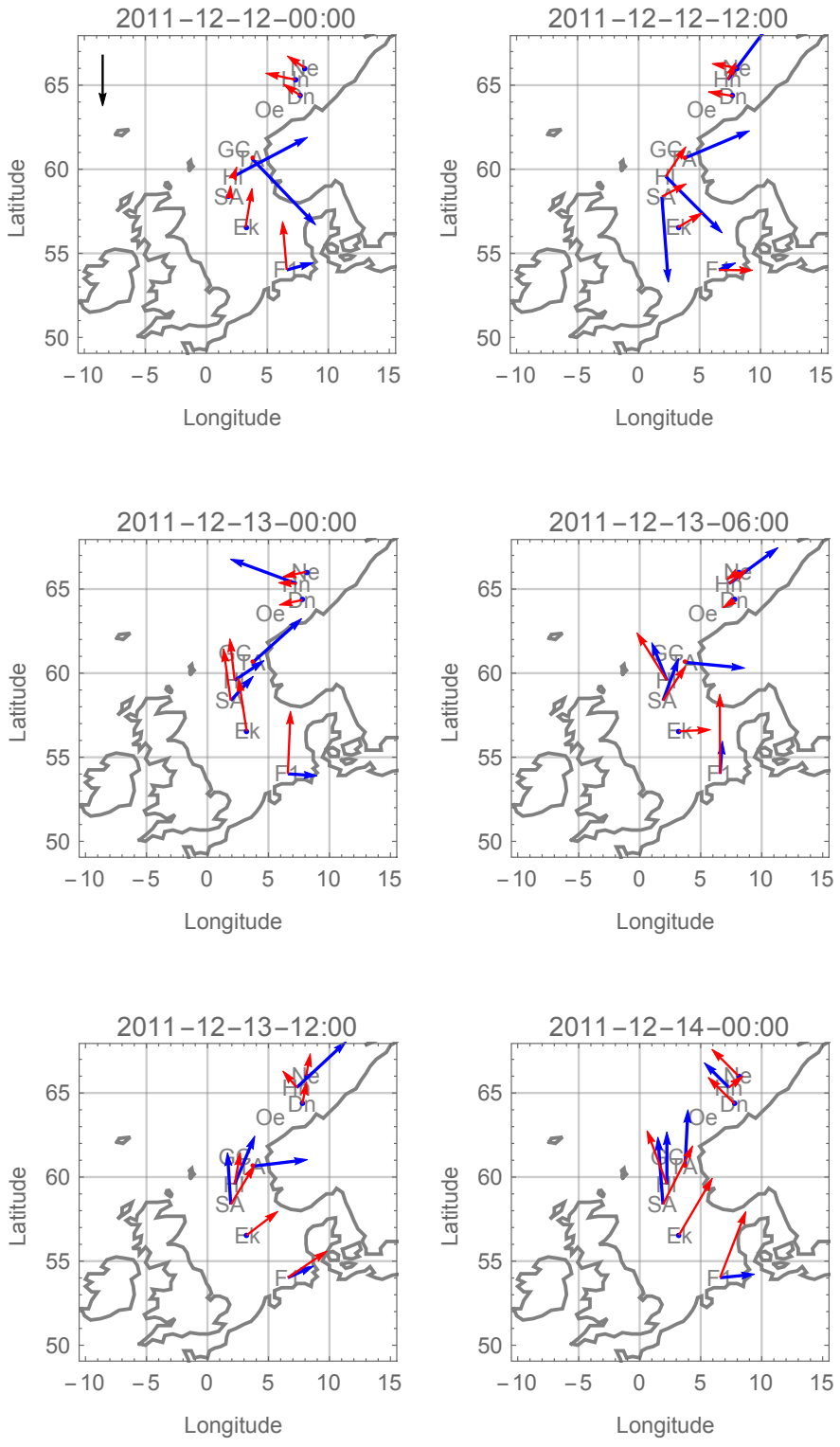

Fig. 14 Similar to Fig. 4. Wind vectors (red arrow) and wave vectors (blue arrows) at stations where data are available during the 2011-Dec storm. The time is printed in the figure labels.

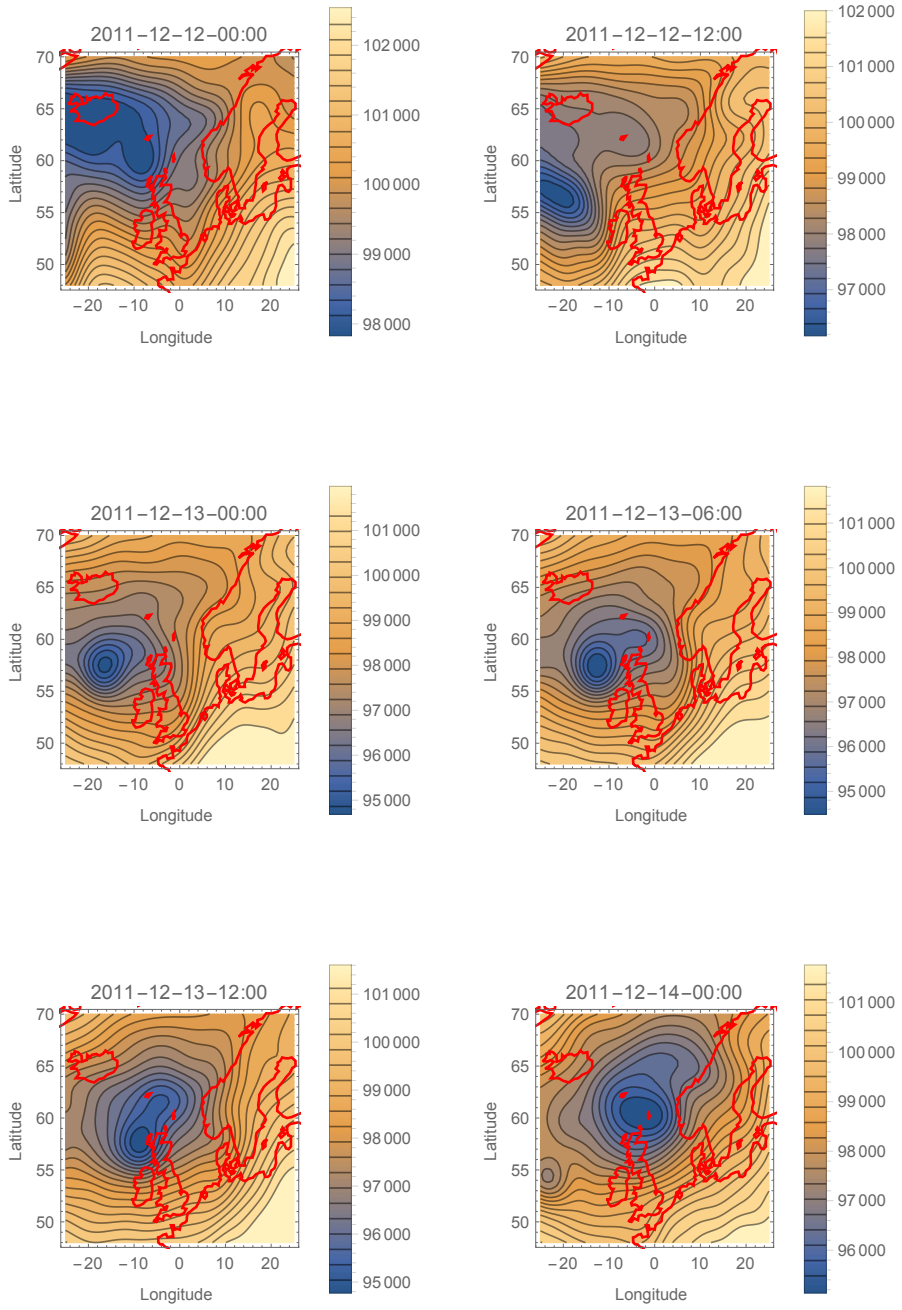

Fig. 15 Isobars during storm Britta, at corresponding time to Fig.14.

.

over the North Sea from afternoon of 2011-11-08 and throughout 2011-11-09 (cf. Fig. 4). The buoy measurements are not available at FINO 1, meaning SST data is not available (see Table 2), but the presence of open cells and the lower temperature at 33 m than at 100 m suggest that the it is of unstable stratification. Thirdly, the SAR image at 10:02 am on 2007-11-09 contains clear open cell structure winds. Overall, it is considered that storm Tilo is similar to Britta.

None of the other storms in the list developed extreme H_s over the North Sea. Corresponding wind and peak wave vectors are calculated with measurements from the 10 stations in the North Sea to track the propagation of the storms in terms of both wind and waves, and to examine the fetches in relation to the wave field propagation. These storms all have relatively strong wind speeds. As shown in Table 2, these storms can correspond to unstable ($T_{air} < SST$), neutral ($T_{air} \approx SST$), or stable ($T_{air} > SST$) conditions. Open cell structures can sometimes be observed from the cloud pictures when $T_{air} < SST$. The CFSR MSLP data are used to allocate the centers of these storms as the position of the minimum MSLP over the domain. It is found that one fact is in common in these storms: the water fetch is often disturbed in the wave propagation direction when wind direction changes within just several hours.

The very unique element in the extreme wave development during Britta that is missing in the other storms examined here (except for Tilo) is the undisturbed water fetch under the impact of strong winds over more than half a day.

4 Discussion

Wind input is one of the most important elements in a successful wave modeling. To accurately capture the storm wind field, here including the open cell structures, numerous tests have been done to find out the optimal WRF model setup, including domain position and size, spatial resolution, initial time of the modeling, simulation length and the choice of SST data. The modeled wind field has shown to be satisfactory.

The nature of a moving front system with fluctuating mean winds associated with open cell structure as in storm Britta might challenge the assumption of stationarity and ergodicity of the wave field as implied in spectral wave modeling (Liu et al 2002). In the wave model, wave spectrum portrays an averaged state of the time frequency energy content of the wave field over a segment of time. Liu et al (2002) pointed out that within this time segment, there are active wave groups which redistribute spectral energy on a continuous basis, and that the processes occurring within the time segment exemplify a critical part of the wind wave dynamics overlooked by current generation of models, including SWAN. As indicated by Donelan et al (1996), the spectral representations for waves in a spectral model preclude unsteady conditions or isolated events. Here, the COAWST modeling system helped us in concluding on the negligible effects from the open cell structures on the measured high values of the significant wave height: H_s at the storm peak was successfully modeled whereas the temporal wind variability related to the open cells is not included in the spectral wave modeling. The two-way online coupling of WRF and SWAN introduces the "mesoscale gustiness" (open cell) systematically into the operational wave forecasting system, overcoming the

technical difficulties as described in Pleskachevsky et al (2012). In the calculation of wind stress through wind speed, as in WRF, it is the classical boundary layer theory that is used. This classical theory assumes zero spectral energy in the time frame between a couple of hours to 10 minutes. Open cell structure contributes non-negligible spectral energy in this range. In SWAN, the wave spectrum covers a frequency range 0.03 Hz to 1.02 Hz, which is a standard setup and it is much higher than the frequency range where the open cells are active (from $f \sim 2 \cdot 10^{-4}$ Hz and higher). It is not immediately clear how the wind fluctuation in this range can be transferred to the wave spectrum. The net impact of the open cell wind structures from the modeling is negligible on the calculation of H_s. Therefore we conclude that the presence of open cells is not a necessary condition for the occurrence of extreme H_s at FINO 1 during Britta. Our analysis of the 2011-Dec storm, with presence of open cells and absence of extreme waves, further suggests that the presence of open cells is not a sufficient condition for the extreme H_s to occur, either. Note the analysis here also differs from Pleskachevsky et al (2012) in that we focus on H_s while Pleskachevsky et al (2012) investigated the resonance effect on the generation of individual rogue wave. Such an effect is not possible to be examined here by the spectral model SWAN.

The similar $H_s - U_{100}$ relation for the 2011-Dec storm as that for the storm Erwin (Emeis and Türk 2009) suggests that the stable condition during Erwin is not sufficient in explaining the difference between Erwin and Britta. Even though the atmospheric stratification affects the air-sea momentum exchange, its effect on the extreme wave development seems secondary.

Several conditions are examined and compared between Britta and a number of storms, including those named in the literatures and those identified here from

FINO 1 measurements. Note that we only analyzed the cases between 2005 and 2013 May here. There are severe storms before and after this period, e.g. storm Anatol in 1999 December and Xaver from 2013 December, which have caused significant storm surge to Northern Europe and huge cost, see such a list in Kristandt et al (2014).

Seemingly, the most important condition that Britta satisfies is the persistent, strong mean wind, with unchanged wind and wave direction during a period of longer than 12 hours over a long undisturbed fetch. The realization of this condition in the North Sea requires the occurrence of a storm path that leaves the long and undisturbed wind and wave fetch over the water. Such conditions are also presented by storm Tilo. No extreme waves developed at FINO 1 during other storms when such conditions are not present.

5 Conclusion

This study overcomes the technical challenges in earlier studies and used an atmosphere-ocean coupled modeling system that is capable of simulating the open cell convection pattern across the North Sea in association with the cold air outbreak of the Britta storm. This approach enables a closer examination of the role of the open cell convection on the development of the extreme H_s during this storm.

Further investigation on the mechanisms of storm Britta has also been made possible through the availability of various types of measurements, including standard meteorological and wave measurements from open sea stations across the North Sea, satellite data and cloud pictures. The investigation has done using

hands full of other storms that are characterized by different conditions combining stability, presence/absence of open cells, storm path and presence/absence of extreme H_s.

The analysis of the wave energy balance equation in SWAN reveals negligible impact of the mesoscale wind fluctuations associated with open cells in the calculation of significant wave height H_s in the current modeling system. COAWST, with WRF and SWAN activated, is capable of capturing important open sea characteristics of a major storm like Britta where extreme waves developed, such as the storm path, storm peak wind speed and significant wave height.

The current study suggests that the necessary conditions for the development of the extreme waves as in storm Britta are primarily: (1) persistent strong mean winds, (2) long and undisturbed fetch during a long period (e.g. 12 hours or more) that allows the development and propagation of strong waves.

Acknowledgements This project is supported by the Danish ForskEL project XWiWa (PSO-12020). We thank Merete Badger for the SAR data, which is provided by the European Space Agency. We thank the EU-Mermaid project for access to the FINO 1 data. CFSR data are obtained from http://rda.ucar.edu/datasets. The cloud pictures are provided by NERC Satellite Receiving Station, Dundee University, Scotland at http://www.sat.dundee.ac.dk. We acknowledge eKlima for the measurements at the 9 stations in the North Sea.

Appendix 1 The T-year return value of H_s

Details of the calculation of the $T-$year return value of H_s can be found in Larsén et al (2015). Briefly, the annual maximum wave height samples are first identified, $H_{s,i}^{max}$, where $i = 1, ..., n$, with n the number of samples:

$$F(X) = \exp\left(-\left(1 - \alpha(X - \beta)\right)\right) \tag{5}$$

Relating $1/T$ to $1-F(X)$ gives the T-year return value for the Gumbel distribution at T as:

$$H_s^T = \alpha^{-1} \ln T + \beta \tag{6}$$

where α and β are obtained with the probability-weighted moment procedure (Abild 1994; Hosking 1985):

$$\alpha = \frac{\ln 2}{2b_1 - \overline{H_s^{max}}}, \quad \beta = \overline{H_s^{max}} - \frac{\gamma_E}{\alpha} \tag{7}$$

where $\gamma_E \approx 0.577216$ is Euler's constant, and $\overline{H_s^{max}}$ is the mean of $H_{s,i}^{max}$. b_1 is calculated from

$$b_1 = \frac{1}{n} \sum_{i=1}^{n} \frac{i-1}{n-1} H_{s,i}^{max} \tag{8}$$

According to Abild (1994) and Hosking (1985), this probability-weighted moment procedure gives less bias and variance on the estimates in comparison with the least square regression method. However, here the calculation is not very different from using the least squares linear regression.

The standard error of the fitting in obtain H_s^T can be calculated from the standard deviation of H_s^{max} (Abild 1994; Mann et al 1998):

$$\sigma(H_s^T) = \frac{\pi}{\alpha} \sqrt{\frac{1 + 1.14 k_T + 1.10 k_T^2}{6n}} \tag{9}$$

where

$$k_T = -\frac{\sqrt{6}}{\pi} \left(\ln\ln \left(\frac{T}{T-1} \right) + \gamma_E \right). \tag{10}$$

The T-year estimate was shown by Kite (1975) to be assumed to be normally distributed. Accordingly, the 95% confidence interval can be estimated to be $1.96 \cdot \sigma(H_s^T)$.

References

Abild J (1994) Application of the wind atlas method to extremes of wind climatology. Tech. Rep. Risoe-R-722(EN), Risø National Laboratory, Roskilde, Denmark

Agee E (1987) Meso-scale cellular convection over the oceans. Dyn Atmos Ocean 10:317–341

Atkinson BW, Zhang JW (1996) Mesoscale shallow convection in the atmosphere. Reviews of Geophysics 4:403–431

Barstow SF, Magnusson AK, Peters D, Krigstad HE (2008) Observations of extreme waves in the long-term measurements at ekofisk. Rogue waves workshop, Brest, October 13-15, http://wwwifremerfr/web-com/stw2008/rw/full/Krogstadpdf

Behrens A, Günther H (2009) Operational wave prediction of extreme storms in Northern Europe. Nat Hazards 49:387–399

Bitner-Gregersen EM, Magnusson AK (2014) Effect of intrinsic and sampling variability on wave parameters and wave statistics. Ocean Dynamics 64:1643–1655

Bolaños R, Larsén XG, Petersen OS, Nielsen JR, Kelly M, H Kofoed-Hansen JD, Sørensen O, Larsen S, Hahmann A, Badger M (2014) Coupling atmosphere and waves for coastal wind turbine design. Conference Proceedings ICCE, 11 pages

Booij N, Ris R, Holthuijsen LH (1999) A third-generation wave model for coastal regions: 1. model description and validation. J Geophys Res doi:101029/98JC02622 104(C4):7649

Brusch S, Lehner S, Schulz-Stellenfleth J (2008) Synergetic use of radar and optial satellite images to support severe storm prediction for offshore wind farming. IEEE Journal of selected topics in applied earth observations and remote sensing 1:57 –66

Brümmer B, Rump B, Kruspe G (1992) A cold air outbreak near spitsbergen in spring time: Boundary layer modification and cloud development. Boundary-Layer Meteorol 61:13 –46

Donelan M, Drennan WM, Magnusson AK (1996) Nonstationarity analysis of the directional properties of propagating waves. J Phys Oceanogr 26:1901–1914

Du J, Larsén XG, Bolaños R (2015) A coupled atmospheric and wave modeling system for storm simulations. Proceedings of EWEA Offshore Conference, Copenhagen

Emeis S, Türk M (2009) Wind-driven wave heights in the German Bight. Ocean Dynamics 59:463–475

Fan Y, Lin S, Held IM, Yu Z, Tolman HL (2012) Global ocean surface wave simulation using a coupled atmosphere-wave model. Journal of Climate 25:6233–6252

Frehlich R, Sharman R (2008) The use of structure functions and spectra from numerical model output to determine effective model resolution. Monthly Weather Rev 136:1537–1553

Gage K, Nastrom G (1986) Theoretical interpretation of atmospheric wavenumber spectra of wind and temperature observed by commercial aircraft during GASP. J Atmos Sci 43:729–740

Hasager C, Badger M, Peña A, Larsén X, Bingöl F (2011) SAR-based Wind Resource Statistics in the Baltic Sea. Remote Sens 3:117–144

Hasager C, Mouche A, Badger M, Bingöl F, Karagali I, Driesenaar T, Stoffelen A, Peña A, Longépé N (2015) Offshore wind climatology based on synergetic use of Envisat ASAR, ASCAT and QuikSCAT. Remote Sensing of Environment 156:247–263

Hersbach H, Stoffelen A, de Haan S (2007) An improved c-band scatterometer ocean geographical model function: Cmod5. J Geophys Res 112:doi:10.1029/2006JC003,743

Hosking J (1985) Estimation of the generalized extreme value distribution by the method of probability-weighted moments. Technometrics 27:251–261

Iacono MJ, Delamere JS, Mlawer EJ, Shephard MW, Clough SA, Collins WD (2008) Radiative forcing by long-lived greenhouse gases: Calculations with the AER radiative transfer models. Journal of Geophysical Research 113:13,013

Kain JS, Fritsch JM (1993) Convective parameterization for mesoscale models: The Kain-Fritsch scheme. The representation of cumulus convection in numerical models, Meteor. Monogr. Ameri Meteor Soc 24:165–170

Kettle AJ (2015a) Britta storm in the North Sea and damage to the FINO 1 platform, Nov. 1, 2006. RAVE Research at Alpha Ventus, ID:2827, http://folkuibno/ake043/Presentations/kettle2015_rave_bremerhavenpdf 68

Kettle AJ (2015b) Review Article: Storm Britta in 2006: offshore damage and large waves in North Sea. Nat Hazards Earth Syst Sci Discuss 3:5493–5510

Kettle AJ (2016) Assessing extreme events for energy meteorology: media and scientific publications to track the events of a North Sea storm. Energy Procedia, European Geosciences Union General Assembly 2016, Division Energy, Resources & Environment 97:116–123

Kite GW (1975) Confidence limits for design events. Water Resources Research 11:48–53

Kristandt J, Brecht B, Knaack H (2014) Optimization of empirical storm surge forecast - modeling of huge resolution wind fields. Die Küste 81:301–318

Larsén XG, Ott S, Badger J, Hahmann AH, Mann J (2012) Recipes for correcting the impact of effective mesoscale resolution on the estimation of extreme winds. J Appl Meteorol Climat 51(3):521–533, DOI 10.1175/JAMC-D-11-090.1

Larsén XG, Vincent CL, Larsen S (2013) Spectral structure of the mesoscale winds over the water. Q J R Meteorol Soc 139:685–700, DOI DOI:10.1002/qj.2003

Larsén XG, Kalogeri C, Galanis G, Kallos G (2015) A statistical methodology for the estimation of extreme wave conditions for offshore renewable applications. Renewable Energy 80:205–218

Larsén XG, Larsen SE, Petersen EL (2016) Full-scale spectrum of boundary-layer winds. Boundary-Layer Meteorol 159:349–371

Liu P, Schwab DJ, Jensen R (2002) Has wind-wave modeling reached its limit? Ocean Engineering 29:81–98

Mann J, Kristensen L, Jensen NO (1998) Uncertainties of extreme winds, spectra and coherences. In: Larsen, Esdahl (eds) Bridge Aerodynamics, ISBN 9054109610, Rotterdam, Balkema

Nakanishi M, Niino H (2009) Development of an improved turbulence closure model for the atmospheric boundary layer. J Meteorol Soc Jpn 87:895–912

Nastrom G, Gage K (1985) A climatology of atmospheric wavenumber spectra of wind and temperature observed by commercial aircraft. J Atmos Sci 42:950–960

Pleskachevsky A, Lehner S, Rosenthal W (2012) Storm observations by remote sensing and influences of gustiness on ocean waves and on generation of rogue waves. Ocean Dynamics 62:1335–1351, DOI 10.1007/s10236-012-0567-z

Saha S, Moorthi S, Pan H, Wu X, et al (2010) The NCEP climate forecast system reanalysis. American Meteorological Society, BAMS pp ES9–ES25, DOI 10.1175/2010BAMS3001.1

Schneggenburger C, Günther H, Rosenthal W (2002) Spectral wave modeling with non-linear dissipation: validation and applications in a coastal tidal enviroment. Coast Eng 41:201–235

Senet C, Fischer J, Outzen O, Herklotz K, Klein H (2012) Remote sensing and in situ sea state instrument comparisons at the research platform FINO 1 in the German Bight. Geoscience and Remote Sensing Symposium (IGARSS), IEEE International pp 7625–7628

Skamarock W (2004) Evaluating mesoscale NWP models using kinetic energy spectra. Mon Weather Rev 132:3019–3032

Thompson G, Rasmussen RM, Manning K (2004) Explicit forecasts of winter precipitation using an improved bulk microphysics scheme. Part-I: Description and sensitivity analysis. Mon Weather Rev 132:519–542

Valenzuela G (1978) Theories for the interaction of electromagnetic and ocean waves - a review. Boundary-Layer Meteorology 13:61–85

Warner JC, Armstrong B, He R, Zambon J (2010) Development of a coupled ocean-atmosphere-wave-sediment transport (COAWST) modeling system. Ocean Modeling 35:230–244

Zijlema M, Vledder GPV, Holthuijsen LH (2012) Bottom friction and wind drag for wave models. Coastal Engineering 65:19–26